Ultrafast Formation of a Charge Density Wave State in 1T-TaS_2: Observation at Nanometer Scales Using Time-Resolved X-Ray Diffraction

C. Laulhé,[1,2,*] T. Huber,[3] G. Lantz,[4,3] A. Ferrer,[5] S. O. Mariager,[5] S. Grübel,[5] J. Rittmann,[5] J. A. Johnson,[5] V. Esposito,[5] A. Lübcke,[5,†] L. Huber,[3] M. Kubli,[3] M. Savoini,[3] V. L. R. Jacques,[4] L. Cario,[6] B. Corraze,[6] E. Janod,[6] G. Ingold,[5] P. Beaud,[5] S. L. Johnson,[3] and S. Ravy[4]

[1]*Synchrotron SOLEIL, L'Orme des Merisiers, Saint Aubin—BP 48, F-91192 Gif-sur-Yvette, France*
[2]*Université Paris-Saclay (Université Paris-Sud), F-91405 Orsay Cedex, France*
[3]*Institute for Quantum Electronics, Physics Department, ETH Zurich, CH-8093 Zurich, Switzerland*
[4]*Laboratoire de Physique des Solides, Université Paris-Sud, CNRS, UMR 8502, F-91405 Orsay, France*
[5]*Swiss Light Source, Paul Scherrer Institute, CH-5232 Villigen, Switzerland*
[6]*Institut des Matériaux Jean Rouxel—UMR 6502, Université de Nantes, 2 rue de la Houssinière, F-44322 Nantes, France*

(Received 22 March 2017; revised manuscript received 28 April 2017; published 16 June 2017)

Femtosecond time-resolved x-ray diffraction is used to study a photoinduced phase transition between two charge density wave (CDW) states in 1T-TaS_2, namely the nearly commensurate (NC) and the incommensurate (I) CDW states. Structural modulations associated with the NC-CDW order are found to disappear within 400 fs. The photoinduced I-CDW phase then develops through a nucleation and growth process which ends 100 ps after laser excitation. We demonstrate that the newly formed I-CDW phase is fragmented into several nanometric domains that are growing through a coarsening process. The coarsening dynamics is found to follow the universal Lifshitz-Allen-Cahn growth law, which describes the ordering kinetics in systems exhibiting a nonconservative order parameter.

DOI: 10.1103/PhysRevLett.118.247401

Strongly correlated electron systems are known to exhibit rich phase diagrams [1–3]. Such compounds also display fascinating out-of-equilibrium physics, in the form of ultrafast symmetry changes known as photoinduced phase transitions [4–6], and occurrence of new, transient states [6–8]. Charge density wave (CDW) states are broken symmetry states of metals arising from electron-phonon interactions. They are characterized by a periodic modulation of both atomic positions and electron density. The metal-to-CDW phase transition is characterized by the growth of a complex-valued order parameter $p = A\exp^{i\Phi}$, which reflects both the amplitude A and the phase Φ of the periodic modulation [3]. A number of photoinduced phase transitions that have been achieved in CDW compounds correspond to a suppression of the CDW order, i.e., a transition between a CDW state and a metallic state free of any structural modulation [5,9–15]. Among those, the photoinduced suppression of the CDW state in blue bronze was shown to involve a coherent motion of atoms along the normal coordinates of the CDW amplitude mode [5]. In this case, the amplitude mode allows continuous variations of the modulus of the order parameter $|p|$, the metallic state corresponding to $|p| = 0$. In the present Letter, we focus on the photoinduced phase transition between the nearly commensurate (NC) and the incommensurate (I) CDW states in 1T-TaS_2, which exhibit two distinct order parameters. When thermally induced, this first-order phase transition involves a discontinuous change of atomic positions, and a coexistence of NC and I phase domains over a 3 K range [16,17]. Thus, it is expected that the photoinduced I phase appears through noncoherent atomic motions, by a nucleation and growth process. We report that the photoinduced NC → I phase is completed within 100 ps after laser excitation. At this 100 ps delay, the photoinduced I-CDW phase is found divided into domains with a typical size of 150 Å. Its ordering kinetics could be captured in the form of a coarsening of the domain pattern. To our knowledge, this constitutes the first experimental observation of a coarsening phenomenon on the nanometer and picosecond length and time scales.

1T-TaS_2 is formed by sheets of edge-linked TaS_6 octahedra [Fig. 1(a)]. In the structure of highest symmetry, the Ta atoms form a regular hexagonal lattice. Below 543 K, a transition to the triple-q modulated I-CDW phase occurs. In this phase, an atom which lies at the position $\vec{r}$ of the hexagonal lattice is displaced by the vector $\vec{u}(\vec{r}) = \sum_{i=1}^{3} u_I \vec{e_i} \times \cos(\vec{q_I}^i \cdot \vec{r} + \Phi_I)$. The I-CDW modulation is characterized by its wave vector $\vec{q_I}^1 = 0.283\vec{a^*} + \frac{1}{3}\vec{c^*}$ and equivalents by the threefold symmetry [17], as well as by the order parameter $p_I = u_I \exp^{i\Phi_I}$ [19] [p. 175]. Below 350 K, the modulation wave vectors suddenly rotate in the $(\vec{a^*}, \vec{b^*})$ plane, marking the onset of the NC-CDW state. At 300 K, the NC phase exhibits modulation vectors $\vec{q_{NC}}^1 = 0.245\vec{a^*} + 0.068\vec{b^*} + \frac{1}{3}\vec{c^*}$ and equivalents by the threefold symmetry [17,20].

The advent of setups dedicated to time-resolved diffraction on sub-ps timescales has allowed detailed analyses

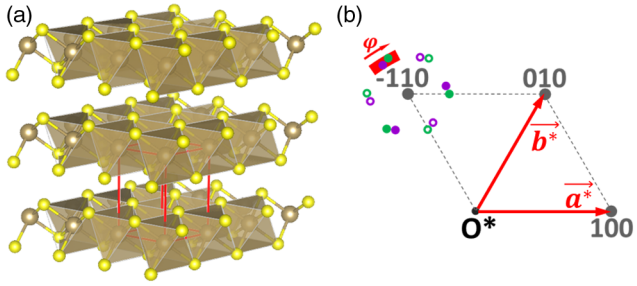

FIG. 1. (a) Crystal structure of $1T$-TaS_2. The hexagonal unit cell is represented in red [18]. (b) Location of diffracted intensity in reciprocal space. Satellite peaks related to the $\bar{1}10$ lattice peak are represented in purple for the NC phase and in green for the I phase (filled circles: $l = \frac{1}{3}$, open circles: $l = -\frac{1}{3}$). Scanning the azimuthal angle φ allows measuring diffracted intensity along the thick red line.

on the mechanism of several photoinduced phase transitions [5–7,10,12,21–23]. Diffraction techniques are especially well adapted to studying CDW compounds [5,10,12,14,15,22,24–29]. Indeed, a structural modulation with wave vector $\vec{q}$ gives rise to satellite peaks [Fig. 1(b)], the intensity of which being proportional to the square of the atomic displacement amplitude $|p|^2$. In this work on $1T$-TaS_2, our original approach consisted in measuring the width of an incipient photoinduced I-CDW satellite peak, inversely proportional to the I-CDW correlation length. Such analyses of time-dependent diffuse scattering signals have rarely been performed, despite their relevance to studying short-range correlated structural features [30].

Femtosecond pump-probe diffraction experiments were carried out using a hard x-ray synchrotron slicing source [31]. A plateletlike, (001)-oriented $1T$-TaS_2 single crystal [32] was excited with 1550 nm laser pulses with p polarization, at an incidence angle of 10° with respect to the surface plane. The diffraction was studied in a grazing incidence geometry by using 7.05 keV, 140 fs x-ray pulses at an incidence angle of about 1°. The effective penetration depths of the laser and x-ray beams are estimated to $\delta_L =$ 44 nm and $\delta_{RX} = 130$ nm, respectively [33,34]. The diffraction condition was tuned by rotating the sample about its surface normal. In the following, this rotation is referred to as the azimuthal angle and denoted φ. The temperature was controlled between 240 and 300 K by means of a N_2 blower.

Figure 2(a) shows the profiles of diffracted intensity measured at the $\vec{q}_{\mathrm{NC}} = (-1.313, 1.245, 0.333)$ and $\vec{q}_{\mathrm{I}} = (-1.283, 1.283, 0.333)$ satellite peak positions in reciprocal space, for various time intervals after photoexcitation (6.8 mJ/cm^2 [35], 265 K). The time dependence of the integrated intensity and full width at half maximum (FWHM) was determined for both satellite peaks, by fitting a pseudo-Voigt function to the data [Fig. 2(b)]. The photoinduced NC → I phase transition is revealed, following a three-step mechanism [Fig. 2(c)]: (1) An ultrafast transition occurs in

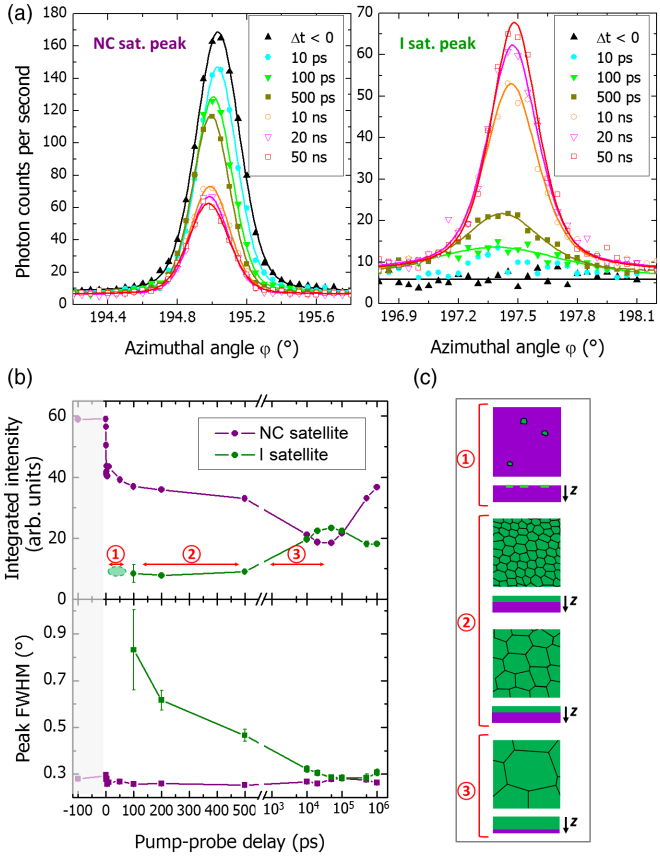

FIG. 2. (a) Diffracted intensity profiles measured at the NC and I satellite peak positions during the NC → I photoinduced phase transition of $1T$-TaS_2 (absorbed fluence 6.8 mJ/cm^2, 265 K). The dots represent measured data and the solid lines their best fit using a pseudo-Voigt function. (b) Time dependence of the NC and I peak profile parameters, as extracted from the fit. (c) Schematic drawing of the three-step dynamics of the photoinduced NC → I phase transition. For each step, crystal views from both the top and the side are given.

the first few ps after laser excitation, as shown by the drop of the NC satellite peak intensity and the concomitant appearance of diffuse scattering at the I satellite peak position. (2) For pump-probe delays ranging from 100 to 500 ps, the integrated intensities of the NC and I satellite peaks remain fairly constant, meaning that the modulation amplitudes and the relative volumes of both phases are stabilized. The width of the I satellite peak, however, still evolves, giving evidence for structural rearrangements within the photoinduced I-CDW state. (3) A second growth of the I phase at the expense of the NC phase is observed at pump-probe delays longer than 500 ps and up to 50 ns. Taking into account the typical heat diffusivity in solids [10^{-6} m^2 s^{-1}] and the 130 nm probed depth, the latter timescales can be associated with heat diffusion processes. Because of the limited penetration depth of the infrared photons, the laser excitation density decays exponentially within the probed depth of the sample [Fig. 3(c)]. Thus, the photoinduced I phase is expected to nucleate close to the sample's surface. Beyond

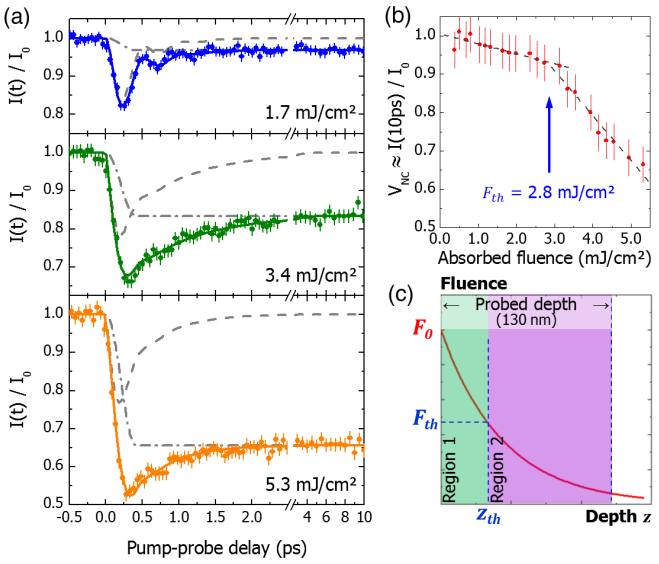

FIG. 3. (a) Time evolution of the normalized diffracted intensity at the NC satellite peak position -1.313, 1.245, 0.333 (240 K). Lines represent the best fits using a weighted sum of the model functions defined for regions 1 and 2 (see text). (b) Relative change of intensity observed for the NC satellite peak as a function of fluence ($\Delta t = 10$ ps). (c) Schematic representation of the inhomogeneous excitation across the probed depth of the $1T$-TaS_2 crystal. The z axis lies normal to the crystal's surface.

100 ps after laser excitation, an effective local temperature can be defined, which follows an in-depth profile similar to that of laser excitation density. Temperature homogeneity is then slowly restored through heat diffusion, which causes a transient temperature increase in the furthest regions from the surface and, in turn, a thermally activated growth of the I phase towards the sample's depth.

Figure 3(a) shows the time evolution of diffracted intensity at the NC satellite peak position $q_{\mathrm{NC}}^{\rightarrow}$ (240 K, 1.7 to 5.3 mJ/cm^2). A drop of diffracted intensity is observed, followed by a partial recovery within 3 ps. The diffracted intensity then remains approximately constant up to at least 10 ps. At the lowest fluence studied, periodic oscillations could be clearly resolved within 2 ps after laser excitation. Variations of the NC satellite peak intensity can reflect either a change of the NC-CDW modulation amplitude, or a change of the relative volume of the NC phase. Figure 2(a) shows that 10 ps after laser excitation, the reduced intensity of the NC satellite peak is observed concomitant with a diffraction contribution located at the I satellite peak position. For larger pump-probe delays, the NC and I satellite peak intensities show an inverse correlation [Fig. 2(b)]. These observations suggest that the intensity variations observed beyond 10 ps after laser excitation are due to changes of the relative volumes of the NC and photoinduced I phases, rather than a change of the NC or I order parameters. Under this assumption, the NC satellite peak intensity at a 10 ps pump-probe delay is a measure of the relative volume of the NC phase. We write $V_{\mathrm{NC}} \approx I(10\ \mathrm{ps})/I_0$, where I_0 denotes the diffracted intensity before laser excitation. Its fluence dependence is reported in Fig. 3(b), giving evidence for two different regimes of the photoinduced response. Below the threshold fluence $F_{\mathrm{th}} = 2.8$ mJ/cm^2, V_{NC} slowly decreases with fluence, but remains greater than 93%. The slope then dramatically increases above F_{th}. We propose that F_{th} is the threshold fluence of the photoinduced NC $\rightarrow$ I phase transition [12].

Assuming linear absorption, the effective laser fluence decays exponentially across the probed depth z, following $F(z) = F_0 e^{-z/\delta_L}$. In the case where $F_0 > F_{\mathrm{th}}$, the sample splits into two regions, each exhibiting a different behavior upon laser excitation [Fig. 3(c)].

Region 1 $[z < z_{\mathrm{th}} = \delta_L \ln(F_0/F_{\mathrm{th}})]$.—This region undergoes the photoinduced NC $\rightarrow$ I phase transition. The NC satellite peak intensity measured from this region is expected to drop to zero within a few ps, as a result of both a decrease of the NC order parameter and a reduction of the relative volume of the NC phase. We chose to model the disappearance of the NC satellite peak intensity by a sigmoid-shaped function. One writes $I_1(t)/I_{1_0} = S(t)$, where $S(t)$ equals $\frac{1}{2}(1 + \cos[\pi t/T_s])$ when $0 \le t \le T_s$, and 0 when $t > T_s$. T_s is the completion time of suppression of the NC-CDW order in region 1.

Region 2 $[z > z_{\mathrm{th}}]$.—No photoinduced transition occurs in this region. In the low fluence regime, laser pulses are known to coherently excite the amplitude mode of the NC-CDW [36–38], which results in periodic oscillations of the modulus of the order parameter p_{NC} in time. This behavior can be modeled assuming a displacive excitation mechanism [5,39]. For $t \ge 0$, one writes $I_2(t)/I_{2_0} = (1 + A_d[\cos(2\pi\nu_{\mathrm{AM}}t)e^{-t/\tau_{\mathrm{AM}}} - e^{-t/\tau_d}])^2$, where A_d, ν_{AM} and τ_{AM} represent the amplitude, frequency, and damping time of the coherent oscillations of the amplitude mode (AM). The time constant τ_d characterizes the relaxation of the transient quasiequilibrium atomic positions.

The function $(1 - V_{\mathrm{NC}})[I_1(t)/I_{1_0}] + V_{\mathrm{NC}}[I_2(t)/I_{2_0}]$ allows an excellent fit of the experimental data [Fig. 3(a)]. In sample parts subjected to a fluence lower than F_{th}, the coherently excited amplitude mode is found to exhibit a frequency ν_{AM} of 1.9 ± 0.2 THz and a short damping constant (τ_{AM} varies from 290 to 140 fs as F_0 increases from 1.7 to 5.3 mJ/cm^2). The parameter τ_d is found equal to 570 ± 200 fs at all fluences studied. These results are consistent with those previously obtained using time-resolved optical measurements and angle-resolved photoemission spectroscopy [36–38]. On the other hand, in sample parts subjected to a fluence higher than F_{th}, the fit using the $S(t)$ function shows that NC modulations decrease within $T_s = 400$ fs, slower than half a period of the NC-CDW amplitude mode [Fig. 3(c)]. A plausible scenario behind this observation could be a displacive excitation of an overdamped amplitude mode [22].

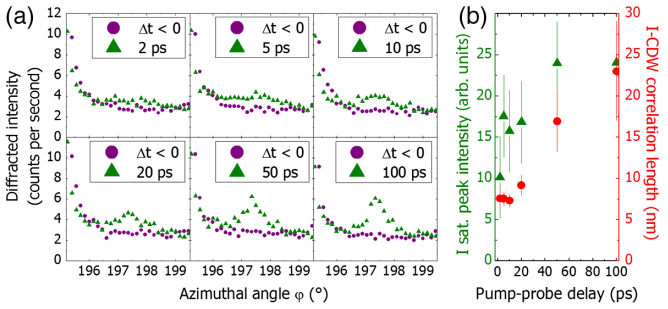

FIG. 4. (a) Diffraction profiles of the photoinduced I satellite peak ($F = 6.8$ mJ/cm^2, $T = 240$ K). The strong contribution observed on the small angle side corresponds to the edge of the NC satellite peak. (b) Time evolutions of the integrated intensity of the I satellite peak (triangular dots), and of the photoinduced I-CDW correlation length (round dots).

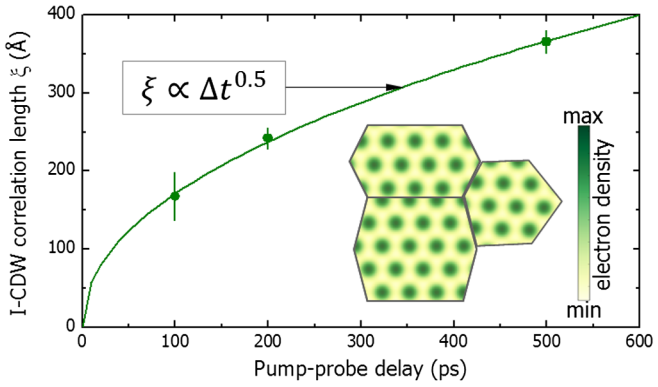

FIG. 5. (dots) Time evolution of the correlation length of the photoinduced I-CDW phase ($F = 6.9$ mJ/cm^2, $T = 265$ K). (line) Best fit using the power law function $C \times \Delta t^{0.5}$. The bottom right inset represents a subset of 3 I-CDW domains, each characterized by a different CDW phase Φ_{In}. Modulations of electronic density associated with the I-CDW are color coded within each of the three domains. For the sake of simplicity, sharp domain walls are represented: their actual width cannot be deduced from the present experiment.

Figure 4(a) shows x-ray diffraction profiles of the I satellite peak, measured at various delays after laser excitation (6.8 mJ/cm^2, T = 240 K). Their angular FWHMs (∼1.7° and ∼0.6° at $\Delta t = 2$ and 100 ps, respectively) are found to be remarkably larger than those of the NC satellite peaks [∼0.3°, see Fig. 2(b)] and regular lattice peaks (∼0.3°, data not shown). In the geometry used for our diffraction experiment, the broadening of the I satellite peak $\Delta\varphi_{\mathrm{I}}$ [40] is related to the spread of diffracted intensity along the $[\vec{a^*} + \vec{b^*}]$ direction [see Fig. 1(b)]: $\Delta q_{\mathrm{I}} \approx \|\vec{q_{\mathrm{I}}} - \frac{1}{3}\vec{c^*}\| \Delta\varphi_{\mathrm{I}}$. Δq_{I} finally translates into the correlation length of the photoinduced I-CDW in the $(\vec{a}, \vec{b})$ plane, following $\xi_{\mathrm{I}} = 2\pi/\Delta q_{\mathrm{I}}$. It is found to increase from 7 to 23 nm in the [2–100 ps] delay range [Fig. 4(b)]. In parallel, we estimated the integrated intensity of the photoinduced I satellite peaks by summing the positive count differences $I(t) - I(t < 0)$ over the φ-angle range [Fig. 4(b)]. The diffracted intensity is found to progressively increase in the pump-probe delay range [2–100 ps], indicating an increase of the photoinduced I phase volume. The concomitant growth of correlation length and increase of the I phase volume observed is fully compatible with the expected scenario of a first order phase transition, where nuclei of the new phase are produced and grow over time.

Now, let us have a closer look at the experimental data presented in Fig. 2(b) (6.9 mJ/cm^2, T = 265 K). In the pump-probe delay range [100–500 ps], the progressive reduction of the I satellite peak FWHM is still observed, meaning that the correlation length of the I-CDW is still increasing. On the other hand, the integrated intensity of the I satellite peak remains constant, meaning that the volume of the photoinduced I phase is stabilized. These observations exclude a scenario where the growth of correlation length would be due to the growth of I phase regions. Instead, the growth of correlation length should be thought of as an internal rearrangement within the photoinduced I-CDW phase. The correlation length of the I-CDW state is a measure of the typical distance over which the phase of the modulation remains constant. Thus, we assume that the photoinduced I phase is fragmented into small domains, each exhibiting one phase Φ_{In} (see inset in Fig. 5).

In the time interval [100–500 ps] after laser excitation, both the electron and phonon energy distributions are expected to be thermalized with a single characteristic local temperature $T(z)$. The observed development of the I phase beyond 100 ps pump-probe delay gives evidence that $T(z)$ is greater than the critical temperature of the NC → I phase transition, at least for some depths z close to the sample's surface [41]. As a consequence, the free energy is well minimized within each photoinduced I-CDW domain. In principle, the phases Φ_{In} can take any value, owing to the incommensurability of the I-CDW with the underlying hexagonal lattice. Nevertheless, the steep change in the I-CDW phase which occurs through the domain walls increases the energy of the system. This leads to a coarsening of the domain pattern, driven by a reduction of the domain wall area [Fig. 2(c), thumbnail 2].

Coarsening systems are known to obey the dynamic scaling hypothesis [42]. Under such an assumption, the domain pattern at later times exhibits similar length distributions as at earlier times, provided that a global scale factor is applied. As a consequence, the time-dependent growth of the domains has to be modeled by a scale-invariant power law At^p. Figure 5 shows the time evolution of the I-CDW correlation length in the [100–500 ps] delay range, as deduced from the broadening of the I satellite peak. The time-dependent power law allows an excellent fit of the data, the refined value for the exponent p being 0.47 ± 0.03. The coarsening dynamics of the photoinduced I-CDW is found to follow the universal Lifshitz-Allen-Cahn growth law ($t^{1/2}$), which describes domain

growth in systems where the order parameter is not conserved [42]. Note that this behavior has seldom been observed experimentally, exclusively on quenched liquid crystals until now, on micrometer and second length and time scales [43,44].

In summary, we depicted the photoinduced NC → I phase transition in $1T$-TaS_2, over the relevant range of timescales [100 fs–1 μs]. The NC-CDW modulations are found to completely disappear within 400 fs. Regions exhibiting I-CDW modulations nucleate and grow within the first 100 ps after laser excitation. At longer pump-probe delays ($\geq$ 100 ps), the photoinduced I phase has fully developed close to the sample's surface. Nonetheless, it does not correspond to the I phase observed at thermodynamic equilibrium: its short correlation length (∼15 nm) makes it a genuine out-of-equilibrium state. Some of the photoinduced nanometric domains grow at the expense of others, in a coarsening process driven by a reduction of the domain wall area. The present work calls for further studies on the fast domain wall dynamics in broken-symmetry phases, which has important implications on the mechanisms of (photoinduced) phase transitions, as well as on material responses to external fields or stimuli.

We wish to warmly thank Sabrina Salmon for her valuable help during sample synthesis, as well as Daniel Grolimund for sharing his expertise during beam line alignment operations. The time-resolved x-ray diffraction measurements were performed on the X05LA beam line at the Swiss Light Source, Paul Scherrer Institut, Villigen, Switzerland. Preparative static grazing incidence diffraction measurements were performed at the CRISTAL beam line of SOLEIL synchrotron, Saint-Aubin, France. The research leading to these results has received funding from the European Community's Seventh Framework Programme (No. FP7/2007-2013) under Grant Agreement No. 312284 (CALIPSO).

*Corresponding author.
laulhe@synchrotron-soleil.fr
†Present address: Max-Born Institute for Nonlinear Optics and Short Pulse Spectroscopy, Max-Born-Strasse 2A, 12489 Berlin, Germany.

[1] E. Dagotto, Rev. Mod. Phys. **66**, 763 (1994).
[2] M. Imada, A. Fujimori, and Y. Tokura, Rev. Mod. Phys. **70**, 1039 (1998).
[3] G. Grüner, *Density Waves in Solids* (Addison-Wesley Publishing Company, Reading, MA, 1994).
[4] P. Beaud, S. L. Johnson, E. Vorobeva, U. Staub, R. A. DeSouza, C. J. Milne, Q. X. Jia, and G. Ingold, Phys. Rev. Lett. **103**, 155702 (2009).
[5] T. Huber, S. O. Mariager, A. Ferrer, H. Schäfer, J. A. Johnson, S. Grübel, A. Lübcke, L. Huber, T. Kubacka, C. Dornes, C. Laulhé, S. Ravy, G. Ingold, P. Beaud, J. Demsar, and S. L. Johnson, Phys. Rev. Lett. **113**, 026401 (2014).
[6] A. Cavalleri, C. Tóth, C. W. Siders, J. A. Squier, F. Ráksi, P. Forget, and J. C. Kieffer, Phys. Rev. Lett. **87**, 237401 (2001).
[7] P. Baum, D.-S. Yang, and A. H. Zewail, Science **318**, 788 (2007).
[8] G. Lantz, B. Mansart, D. Grieger, D. Boschetto, N. Nilforoushan, E. Papalazarou, N. Moisan, L. Perfetti, V. Jacques, D. L. Bolloch, C. Laulhé, S. Ravy, J.-P. Rueff, T. Glover, M. Hertlein, Z. Hussain, S. Song, M. Chollet, M. Fabrizio, and M. Marsi, Nat. Commun. **8**, 13917 (2017).
[9] F. Schmitt, P. Kirchmann, U. Bovensiepen, R. Moore, L. Rettig, M. Krenz, J.-H. Chu, N. Ru, L. Perfetti, D. Lu, M. Wolf, I. Fisher, and Z.-X. Shen, Science **321**, 1649 (2008).
[10] M. Eichberger, H. Schäfer, M. Krumova, M. Beyer, J. Demsar, H. Berger, G. Moriena, G. Sciaini, and R. J. D. Miller, Nature (London) **468**, 799 (2010).
[11] T. Rohwer, S. Hellmann, M. Wiesenmayer, C. Sohrt, A. Stange, B. Slomski, A. Carr, Y. Liu, L. Avila, M. Kalläne, S. Mathias, L. Kipp, K. Rossnagel, and M. Bauer, Nature (London) **471**, 490 (2011).
[12] E. Möhr-Vorobeva, S. L. Johnson, P. Beaud, U. Staub, R. De Souza, C. Milne, G. Ingold, J. Demsar, H. Schaefer, and A. Titov, Phys. Rev. Lett. **107**, 036403 (2011).
[13] S. Hellmann, T. Rohwer, M. Kalläne, K. Hanff, C. Sohrt, A. Stange, A. Carr, M. Murnane, H. Kapteyn, L. Kipp, M. Bauer, and K. Rossnagel, Nat. Commun. **3**, 1069 (2012).
[14] N. Erasmus, M. Eichberger, K. Haupt, I. Boshoff, G. Kassier, R. Birmurske, H. Berger, J. Demsar, and H. Schwoerer, Phys. Rev. Lett. **109**, 167402 (2012).
[15] P. Zhu, J. Cao, Y. Zhu, J. Geck, Y. Hidaka, S. Pjerov, T. Ritschel, H. Berger, Y. Shen, R. Tobey, J. P. Hill, and X. J. Wang, Appl. Phys. Lett. **103**, 071914 (2013).
[16] J. V. Landuyt, Physica (Amsterdam) **99B+C**, 12 (1980).
[17] T. Ishiguro and H. Sato, Phys. Rev. B **44**, 2046 (1991).
[18] K. Momma and F. Izumi, J. Appl. Crystallogr. **44**, 1272 (2011).
[19] K. Motizuki, *Structural Phase Transitions in Layered Transition-Metal Compounds* (D. Reidel Publishing Company, Dordrecht, 1986).
[20] A. Spijkerman, J. L. de Boer, A. Meetsma, G. A. Wiegers, and S. van Smaalen, Phys. Rev. B **56**, 13757 (1997).
[21] P. Beaud *et al.*, Nat. Mater. **13**, 923 (2014).
[22] K. Haupt, M. Eichberger, N. Erasmus, A. Rohwer, J. Demsar, K. Rossnagel, and H. Schwoerer, Phys. Rev. Lett. **116**, 016402 (2016).
[23] S. O. Mariager, F. Pressacco, G. Ingold, A. Caviezel, E. Möhr-Vorobeva, P. Beaud, S. L. Johnson, C. J. Milne, E. Mancini, S. Moyerman, E. E. Fullerton, R. Feidenhansl, C. H. Back, and C. Quitmann, Phys. Rev. Lett. **108**, 087201 (2012).
[24] T.-R. T. Han, Z. Tao, S. D. Mahanti, K. Chang, C.-Y. Ruan, C. D. Malliakas, and M. G. Kanatzidis, Phys. Rev. B **86**, 075145 (2012).
[25] C. Laulhé, L. Cario, B. Corraze, E. Janod, T. Huber, G. Lantz, S. Boulfaat, A. Ferrer, S. O. Mariager, J. A. Johnson, S. Grübel, A. Lübcke, G. Ingold, P. Beaud, S. L. Johnson, and S. Ravy, Physica (Amsterdam) **460B**, 100 (2015).
[26] A. Singer, M. J. Marsh, S. H. Dietze, V. Uhlíř, Y. Li, D. A. Walko, E. M. Dufresne, G. Srajer, M. P. Cosgriff, P. G. Evans, E. E. Fullerton, and O. G. Shpyrko, Phys. Rev. B **91**, 115134 (2015).

[27] S. Sun, L. Wei, Z. Li, G. Cao, Y. Liu, W. J. Lu, Y. P. Sun, H. Tian, H. Yang, and J. Li, Phys. Rev. B **92**, 224303 (2015).
[28] R. G. Moore *et al.*, Phys. Rev. B **93**, 024304 (2016).
[29] A. Singer, S. K. K. Patel, R. Kukreja, V. Uhlíř, J. Wingert, S. Festersen, D. Zhu, J. M. Glownia, H. T. Lemke, S. Nelson, M. Kozina, K. Rossnagel, M. Bauer, B. M. Murphy, O. M. Magnussen, E. E. Fullerton, and O. G. Shpyrko, Phys. Rev. Lett. **117**, 056401 (2016).
[30] L. Guérin, J. Hébert, M. Buron-Le Cointe, S. I. Adachi, S. Y. Koshihara, H. Cailleau, and E. Collet, Phys. Rev. Lett. **105**, 246101 (2010).
[31] P. Beaud, S. L. Johnson, A. Streun, R. Abela, D. Abramsohn, D. Grolimund, F. Krasniqi, T. Schmidt, V. Schlott, and G. Ingold, Phys. Rev. Lett. **99**, 174801 (2007).
[32] S. Ravy, C. Laulhé, J. P. Itié, P. Fertey, B. Corraze, S. Salmon, and L. Cario, Physica (Amsterdam) **407B**, 1704 (2012).
[33] A. Beal, H. Hughes, and W. Liang, J. Phys. C **8**, 4236 (1975).
[34] B. Henke, E. Gullikson, and J. Davis, At. Data Nucl. Data Tables **54**, 181 (1993).
[35] All fluences in this Letter correspond to absorbed fluences, calculated with optical reflectivity data from [33].
[36] J. Demsar, L. Forró, H. Berger, and D. Mihailovic, Phys. Rev. B **66**, 041101 (2002).
[37] L. Perfetti, P. A. Loukakos, M. Lisowski, U. Bovensiepen, H. Berger, S. Biermann, P. S. Cornaglia, A. Georges, and M. Wolf, Phys. Rev. Lett. **97**, 067402 (2006).
[38] L. Perfetti, P. A. Loukakos, M. Lisowski, U. Bovensiepen, M. Wolf, H. Berger, S. Biermann, and A. Georges, New J. Phys. **10**, 053019 (2008).
[39] H. J. Zeiger, J. Vidal, T. K. Cheng, E. P. Ippen, G. Dresselhaus, and M. S. Dresselhaus, Phys. Rev. B **45**, 768 (1992).
[40] Assuming an instrumental width of 0.3°, the broadening is calculated as $\Delta\varphi_I = \sqrt{\mathrm{FWHM}^2 - 0.3^2}$.
[41] $T(z)$ is expected to exhibit a similar z dependence as $F(z)$ [see Fig. 3(c)].
[42] A. J. Bray, Adv. Phys. **51**, 481 (2002).
[43] H. Orihara and Y. Ishibashi, J. Phys. Soc. Jpn. **55**, 2151 (1986).
[44] A. Sicilia, J. J. Arenzon, I. Dierking, A. J. Bray, L. F. Cugliandolo, J. Martínez-Perdiguero, I. Alonso, and I. C. Pintre, Phys. Rev. Lett. **101**, 197801 (2008).